PHYSICAL REVIEW B **92**, 075201 (2015)

Electroreflectance of thin-film solar cells: Simulation and experiment

Christian Huber,* Christoph Krämmer,* David Sperber, Alice Magin, Heinz Kalt, and Michael Hetterich
Institute of Applied Physics, Karlsruhe Institute of Technology (KIT), 76131 Karlsruhe, Germany

(Received 21 April 2015; revised manuscript received 15 June 2015; published 4 August 2015)

Electromodulated reflectance (ER) is a standard characterization method to determine critical points such as the band gap in the band structure of semiconductors. These critical points show up as spectrally narrow features in ER and are typically evaluated using Aspnes's third-derivative functional form. ER spectra of stratified semiconductor systems such as thin-film solar cells, however, are significantly distorted by optical interference due to their layered structure. Furthermore, strong built-in electric fields result in a deviation from the typically assumed low-field conditions. We present here simulations of ER spectra from stratified systems based on transfer matrices using the Franz-Keldysh theory in its general form. For realistic thin-film solar cell conditions, distortions of ER line shapes due to the above-mentioned interferences and strong electric fields appear in the simulations. Furthermore, the results show good agreement with measured ER spectra of a structurally well-characterized Cu(In,Ga)Se_2 (CIGS) solar cell. Our analysis points out the restrictions on the determination of energetic position and number of critical points from ER spectra of stratified systems.

DOI: 10.1103/PhysRevB.92.075201 PACS number(s): 78.20.Ci, 78.66.−w, 88.40.jn

I. INTRODUCTION

Thin-film photovoltaics is seen as a potential successor to silicon photovoltaics due to the better cost efficiency of the solar cell modules. Currently, Cu(In,Ga)$(S,Se)_2$ (CIGS) is the most successful representative of thin-film solar cells with an achieved record power conversion efficiency of 21.7% [1]. An elaborate optimization of solar cell device characteristics generally relies on a detailed knowledge of the physical properties of the materials involved. In particular, the band gap E_g of the absorber layer is one of the most important properties since it determines the absorption edge.

Modulation spectroscopy (MS) has been proven to be a reliable and precise technique to determine critical points in the band structure of bulk semiconductors [2–4] but also of low-dimensional structures such as quantum wells [5–7]. The sharp, derivativelike line shapes in the spectra can be used to resolve even the smallest energetic splittings in semiconductor band structures. Shay *et al.* investigated $CuInSe_2$ [8] and $CuGaSe_2$ [9] single crystals using electroreflectance (ER) and determined band gap and valence band splitting energies which still hold as a reference today. Since such splittings and band gap energies can be used to gain insight into film properties such as strain or alloy composition in the case of, e.g., Cu(In,Ga)$(S,Se)_2$, MS is a promising technique, especially for the characterization of finished thin-film solar cell devices. In particular, the presence of a *p-n* junction is a convenient way to realize a surface barrier ER measurement as described by Aspnes by modulating the built-in electrical field using an ac voltage [10].

ER measurements on solar cells have been performed by Theodoropoulou *et al.* who investigated the strain in the absorber of Cu(In,Ga)S_2 solar cells [11]. ER has furthermore been used to measure band gap shifts in $Cu_2ZnSn(S,Se)_4$ solar cells related to post-annealing [12]. However, ER spectra of solar cells often exhibit oscillations due to interferences which complicate their analysis [11,13].

These complications are caused by several circumstances which make thin-film solar cells a special kind of sample that requires a detailed review of the prerequisites for the evaluation of the resulting spectra. Two of these peculiarities, namely the strong inhomogeneous electric fields in the space charge region (SCR) and the fact that a thin-film solar cell is a dielectric layer stack, are investigated using simulations based on the transfer matrix method (TMM). The discussions are focused on CIGS thin-film solar cells. However, we stress that the results also apply to cells based on other absorbers like, e.g., $Cu_2ZnSn(S,Se)_4$ or thin-film layer systems and devices in general.

The simulations show that the strong intrinsic electric field in the space charge region significantly alters ER spectra. Furthermore, the interference oscillations in the reflection signal due to thin-film interferences lead to oscillations in the respective ER spectra as well. Distortions of ER line shapes appear in the energetic vicinity of interference minima of the reflection signal. The applicability of the TMM to actual solar cells is shown by manually fitting simulation data to a measured ER spectrum of a CIGS solar cell. This allows us to extract the transition energies of the fundamental band gap and the spin-orbit split-off optical transition in the CIGS absorber.

II. THEORY OF ELECTROREFLECTANCE

First, we give an overview of the theoretical background related to this work. The frequency-dependent reflectivity $R(\omega)$ of a medium is determined by its dielectric function $\epsilon(\omega)$. In ER experiments an external voltage is applied to the *p-n* junction, which tilts the band structure and therefore causes a perturbation of the dielectric function. This leads to a change in reflectivity, the normalized quantity $\Delta R/R$ of which is the signal to be measured. It can be expressed as

$$\frac{\Delta R}{R} = a\Delta\epsilon_1 + b\Delta\epsilon_2, \qquad (1)$$

where $\Delta\epsilon_1$ and $\Delta\epsilon_2$ are the changes in the real and imaginary part of the dielectric function, respectively [3]. a and b are the Seraphin coefficients and all quantities are frequency

---

[*] These authors contributed equally.

dependent. While b vanishes for bulk semiconductors at the fundamental absorption edge [14], it has been pointed out that for multilayer structures showing interference effects both Seraphin coefficients have to be taken into account [14–16].

Expressions for $\Delta\epsilon$ in the presence of an electric field F around critical points in the weak-field effective-mass approximation have been developed using Airy functions [17]. These assume parabolic bands and neglect electron-hole interaction. For a M_0 critical point such as the fundamental band gap of a direct semiconductor $\Delta\epsilon$ is given by [18]

$$\Delta\epsilon_2(z) = B\hbar\theta^{1/2}\mathrm{Re}\left[\frac{H(z)}{(\hbar\omega - i\Gamma)^2}\right], \tag{2}$$

$$\Delta\epsilon_1(z) = B\hbar\theta^{1/2}\mathrm{Im}\left[\frac{H(z)}{(\hbar\omega - i\Gamma)^2}\right]. \tag{3}$$

In these expressions, the electro-optic function $H(z)$ is given by

$$\begin{aligned} H(z) = {} & \pi[\mathrm{Ai}'^2(z) - z\mathrm{Ai}^2(z)] \\ & + i\pi[\mathrm{Ai}'(z)\mathrm{Bi}'(z) - z\mathrm{Ai}(z)\mathrm{Bi}(z)] + iz^{1/2}. \end{aligned} \tag{4}$$

The complex argument $z = \frac{E_g - \hbar\omega + i\Gamma}{\hbar\theta}$ includes lifetime-related homogeneous Lorentzian broadening with a broadening parameter Γ. E_g is the respective transition energy. $(\hbar\theta)^3 = \frac{e^2F^2\hbar^2}{2\mu}$ is the electro-optic energy with electron charge e and reduced effective mass μ. Depending on the context in literature, the electro-optic energy is sometimes also defined as $\hbar\Omega = \hbar\theta/\sqrt[3]{4}$ [2]. $\mathrm{Ai}(z)$, $\mathrm{Bi}(z)$, $\mathrm{Ai}'(z)$, and $\mathrm{Bi}'(z)$ are the Airy functions of first and second kind and their first derivatives, respectively. The prefactor B is a constant including, e.g., the transition matrix element.

Equation (1) together with Eqs. (2) and (3) allows us to calculate an ER signal given that the Seraphin coefficients are known. However, simplifications can be made in order to model the line shape, knowing neither $\Delta\epsilon$ nor the Seraphin coefficients and therefore simplifying fitting procedures.

In the case of small perturbations, i.e., low fields, Aspnes introduced the so called third-derivative functional form (TDFF) [2]:

$$\frac{\Delta R}{R} = \mathrm{Re}\left[e^{i\varphi}\frac{A}{(\hbar\omega - E_g + i\Gamma)^n}\right]. \tag{5}$$

In this expression for a so called oscillator, n is determined by the dimensionality of the free electron movement in the medium and $n = \frac{5}{2}$ holds for three dimensions. A and the phase factor $e^{i\varphi}$ are influenced by effects such as electron-hole correlation effects as well as field inhomogeneities and only vary slowly with $\hbar\omega$. E_g and Γ however are independent of these effects and can be found directly from experiment by fitting Eq. (5) to an experimental line shape.

At this point we would like to emphasize the assumptions for the TDFF approximation. First of all, charge carriers are assumed to be free so that they can be accelerated by an electric field. The field itself is assumed to be low. Low means that $|\hbar\Omega|/\Gamma \leqslant 1/3$ (or $|\hbar\theta|/\Gamma \leqslant \sqrt[3]{4}/3$) holds so that the uncertainty in energy gained by the acceleration of the electrons in the electric field is small compared to the lifetime related uncertainty Γ. Finally, TDFF theory in its original form treats only one interface between two media so that it does not take into account interference effects in the reflected light.

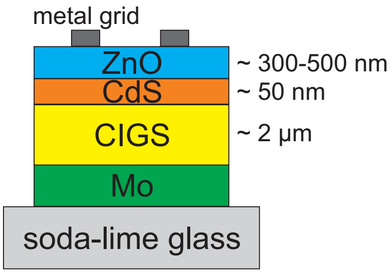

FIG. 1. (Color online) Basic layer stack of a CIGS thin-film solar cell.

CIGS-based thin-film solar cells are typically made of a layer stack as can be seen in Fig. 1. A transparent ZnO window layer is followed by a thin CdS buffer layer and the CIGS absorber layer. The back contact is usually made of Mo. Between each layer there is a strong contrast in refractive index. Therefore, the overall reflectivity shows interference effects. Furthermore, a strong internal field is present at the interface between CIGS and CdS. Depending on the absorber material, trapping of charge carriers in spatial potential or band gap fluctuations of the band structure might also be an issue. Such fluctuations can occur in highly defectuous materials or in the presence of secondary phases as in, e.g., $\mathrm{Cu_2ZnSn(S,Se)_4}$, and cause trapping especially at low temperatures [19]. In this paper we focus on the electrical field and interference effects in ER spectra since these are not specific to the absorber material and can therefore be regarded as valid for thin-film solar cells in general.

As can be seen from the previous discussion, the requirements for the TDFF approximation stand in contrast to the actual situation found in a thin-film solar cell. It is therefore not *a priori* clear that a TDFF analysis is justified for the evaluation of ER spectra taken from thin-film solar cells. In the following, the transfer matrix simulation algorithm used in this paper will be introduced.

III. SIMULATION ALGORITHM

A. General transfer matrix method

The reflectivity of a thin-film solar cell stack was calculated using the method of transfer matrices. In this one-dimensional formalism the electric field amplitudes of waves propagating to the right and to the left are represented by a two-dimensional vector. The evolution of the amplitudes at an interface and the propagation of the electric field through a medium are described by interface and propagation 2 × 2 matrices which are given by [20]

$$M_{ij}^I = \frac{1}{t_{ij}}\begin{pmatrix} 1 & r_{ij} \\ r_{ij} & 1 \end{pmatrix}, \quad M_j^P = \begin{pmatrix} e^{-ik\tilde{n}_j d_j} & 1 \\ 1 & e^{ik\tilde{n}_j d_j} \end{pmatrix}. \tag{6}$$

Here t_{ij} and r_{ij} are the reflection and transmission coefficient at an interface between medium i and j resulting from the Fresnel equations for a wave coming from medium i. k is the wave vector in vacuum, $\tilde{n}_j$ is the complex refractive index of medium j, and d_j its thickness. A N-layer stack can then be described by the matrix product [20]

$$M_{\mathrm{stack}} = M^{I}_{01} M^{P}_{1} M^{I}_{12} M^{P}_{2} \cdots M^{P}_{N} M^{I}_{NN+1} = \begin{pmatrix} T_{11} & T_{12} \\ T_{21} & T_{22} \end{pmatrix}. \tag{7}$$

The reflectivity of the full stack is given by $R = |T_{21}/T_{11}|^2$.

B. Application to CIGS thin-film solar cells

Tabulated refractive index data have been used for Mo [21] and ZnO [22]. A CdS buffer layer has not been taken into account for the simulation, because it would be thinner than the roughness layer between ZnO and CIGS and it is transparent in the spectral region of interest. For CIGS a critical point parabolic band (CPPB) oscillator [16] has been fitted to the absorption edge of the dielectric function measured by Minoura *et al.* [23]. Using the respective fitted values for amplitude, broadening, and offset, the functional form of ϵ around the absorption edge was then shifted to the desired energy for the simulations. We note that in CIGS the valence band maximum is split into three due to spin-orbit interaction and the crystal field so that there are in fact three different contributions to ϵ [24,25]. As described in Sec. II, the presence of an electric field in CIGS distorts the band structure, which leads to a change $\Delta\epsilon$ especially in the energetic vicinity of every critical point. It will however be shown in Sec. V D that the crystal field splitting of our absorbers cannot be resolved in an ER experiment.

The aim of these simulations was to understand the alterations of an ER signal caused by interferences due to a multilayer stack and by the electric field configuration of a thin-film solar cell during measurement. For these simulations, we will therefore work in a simplified picture by only using one optical transition that contributes to $\Delta\epsilon$, i.e., we neglect the valence band splitting. However, we will take the resolvable spin-orbit split-off band into account by a second optical transition for fitting a measured spectrum of a CIGS solar cell.

$\Delta\epsilon$ is then calculated for different field configurations (see Sec. V B) and added to ϵ in order to obtain the perturbed dielectric function in an electric field. At this point we explicitly stress that we used the more general expressions Eqs. (2) and (3) instead of a TDFF expression in order to calculate $\Delta\epsilon$. This way the results obtained are not restricted to the low-field regime. As will be shown in Sec. V A, for a thin-film solar cell, the electro-optic energy is determined by the doping concentration and can exceed low-field conditions for highly doped absorbers.

When evaluating the electro-optic function $H(z)$ in the complex plane, the evaluation of the Airy functions causes divergences for finite imaginary and large real parts of z, i.e., in the case of low fields. However, far away from the critical point an asymptotic expression for $H(z)$ can be used [26]:

$$H(z) \approx \frac{i}{32} z^{-5/2} - \frac{i}{4z} \exp\left(i \frac{4}{3} z^{3/2}\right). \tag{8}$$

In order to decide whether the full expression for $H(z)$ or the asymptotic expression shall be used, a slightly modified version of the empirical boundaries in the complex plane as published by Hall *et al.* was used [27].

C. Laminar approach for inhomogeneous electric fields and interface roughness

There are two approaches in literature to account for inhomogeneous films in ER simulations. Aspnes and Frova showed by using a WKB approximation that for ER an inhomogeneous field can be treated like an effective homogeneous field [28], which in turn has been used for simulations [29]. Other authors used a laminar approach, by discretizing the region of the inhomogeneous field into thin sublayers and setting the field constant in each sublayer [18,30]. There has been some controversy on the reliability of the two approaches [29,31]. Since in our simulations we observed fast convergence of the line shapes with a low number of sublayers of around 20, consistent with Batchelor *et al.* [18], we used the laminar approach for this study. A linear decay of the electric field over the length of the SCR was assumed, consistent with our simulated field distribution presented in Sec. V A.

An optical model such as the one presented above represents a sequence of flat interfaces. At each interface and during propagation through the layers the electromagnetic waves conserve their coherence resulting in interference oscillations with large amplitudes in the reflectivity spectrum. The model is also one dimensional in the sense that the propagation direction is fixed in a material and only changes according to Snell's law at an interface. The calculated reflectivity therefore corresponds to the specular reflectivity measured with identical angle of incidence and angle of detection. For a measurement with a different angle of detection, i.e., diffuse reflection, a transfer matrix model would predict zero reflectivity.

In a real solar cell however, interfaces exhibit surface roughness. Therefore, impinging on such an interface will smear out the phases of the wavefronts and thus damp the interference oscillations. Furthermore, light can scatter out of the direction of propagation because of surface roughness. This leads to a decrease of the specular reflection and an additional diffuse reflection.

In a CIGS solar cell the roughnesses of the layers in terms of the height profile standard deviation are in the order of $\sigma_{\mathrm{rms}} \approx 70$ nm depending on the kind of production process used [32]. The Rayleigh criterion gives a rule of thumb for the classification of a surface as being rough or smooth depending on σ_{rms} and the wavelength λ by calculating the range of phase shifts induced by the roughness:

$$\Delta\varphi = \frac{2\pi n}{\lambda} \sigma_{\mathrm{rms}} \cos\theta \begin{cases} < \frac{\pi}{2} & \text{smooth,} \\ > \frac{\pi}{2} & \text{rough.} \end{cases} \tag{9}$$

Here n is the real part of the refractive index and θ is the angle of incidence. Typical wavelengths in our experiments are of the order of $\lambda \approx 1100$ nm and the index of refraction of ZnO is around $n_{\mathrm{ZnO}} \approx 1.8$. Therefore, e.g., for the air/ZnO interface $\Delta\varphi_{\mathrm{air/ZnO}} \approx 0.34 < \frac{\pi}{2}$ and for the ZnO/CdS interface $\Delta\varphi_{\mathrm{ZnO/CdS}} \approx 0.62 < \frac{\pi}{2}$. Thus, the interfaces can be classified as smooth justifying the coherent treatment of transfer matrices. However, due to the existing roughness the measured specular reflectance can be expected to be lower than in simulations and the interference oscillations to be less pronounced.

It is furthermore known that a $MoSe_2$-rich intermediate layer is formed between CIGS and the Mo back contact [33], which no reliable refractive index data were available for.

In our simulations the roughness-related reduction of specular reflection and the $MoSe_2$-rich layer were treated phenomenologically in a similar manner to the inhomogeneous electric field. Each interface was replaced by a series of thin sublayers with an effective refractive index, calculated from a linear interpolation of the respective adjacent bulk materials. Therefore, $MoSe_2$ was effectively treated as a spatially extended roughness layer between CIGS and Mo. It is mentioned explicitly in Sec. V if rough intermediate layers were used in a specific simulation.

IV. EXPERIMENT

ER spectra of a thin-film solar cell were recorded as follows: Light from a 250-W quartz tungsten halogen lamp was dispersed in a 0.32-m focal-length monochromator with a 600 lines/mm grating. The resulting monochromatic light was then focused onto the sample and the reflected light collected using a lens system. For detection we used either an amplified thermoelectrically cooled InGaAs or Si photodiode. The average photodiode output voltage—proportional to the reflected intensity—was measured using a digital multimeter. A square-wave modulation voltage in reverse bias ($f \approx$ 200 Hz, 0 to −1.8 V) was applied using a function generator. The change in reflected intensity was measured using an analog lock-in amplifier. Data acquisition using a personal computer finally yielded $\Delta R/R$.

External quantum efficiency (EQE) spectra were recorded as follows: Light from a 400-W quartz tungsten halogen lamp was dispersed in a prism monochromator. The emerging light with a narrow bandwidth was then imaged onto the solar cell through a defined aperture. The incident photon flux was monitored using a calibrated germanium photodiode. The light was intensity modulated using an optical chopper wheel and the resulting photocurrent—proportional to the number of extracted generated electron-hole pairs—was converted into a voltage using a transimpedance amplifier the output of which was fed into a lock-in amplifier.

V. RESULTS AND DISCUSSION

A. Electric field configuration in the space charge region

First, the effects of the electric field in the SCR of a thin-film solar cell on ER spectra will be discussed. The spatial distribution of the electro-optic energy $\hbar\theta(x)$ responsible for $\Delta\epsilon$ depends on the electric field distribution $F(x)$ within the *p-n* junction of the solar cell. Since in ER an ac voltage is applied to the device the band structure is tilted and the field distribution is modified. This affects not only the maximum field strength, but also the decay length of the electric field and hence the SCR. In order to determine numeric values for these two quantities, device simulations were performed using SCAPS [34] and typical material parameters as well as layer thicknesses for the device under investigation.

Figure 2 depicts $F(x)$ in the SCR for an absorber acceptor density of $N_A = 5 \times 10^{16}$ cm^{-3} and a buffer donor density of $N_D = 5 \times 10^{17}$ cm^{-3} with and without an applied reverse bias of −2 V. For both voltages, the electric field decays essentially linearly over the largest part of the SCR within the absorber layer. This justifies the use of the Schottky approximation in our TMM simulations, which assumes a linear decay of the electric field over a decay length d_{SCR}—the width of the SCR in the absorber.

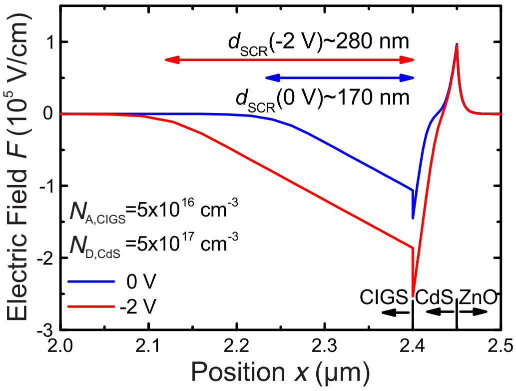

FIG. 2. (Color online) Simulated field distribution within the SCR of the solar cell with (red) and without (blue) reverse bias of −2 V. The electric field decays almost linearly over a large portion of the SCR justifying the use of the Schottky approximation in the optical simulation.

More importantly, d_{SCR} changes depending on the applied bias voltage, which is considered explicitly in our optical simulations. We note that the values for the maximum field strength F_{max} and d_{SCR} strongly depend on the chosen values for the acceptor density N_A within the CIGS layer.

At this point we would like to emphasize that the depth of information in ER measurements is limited to the SCR of the solar cell. In order for a signal to arise, a modulation of the built-in potential has to occur which is only the case for the buffer-absorber interface region as can be seen explicitly in Fig. 3. Therefore, inhomogeneities of the absorber outside the SCR which affect the band structure like, e.g., a gradient in the gallium content, cannot affect an ER spectrum.

B. Electric field effects in electroreflectance spectra

In the original derivation of the TDFF line shape by Aspnes, reflection at a single interface and modulation of the semiconductor from zero field, i.e., flat-band conditions are considered [2]. The externally applied electric field is uniform and fulfils the low-field conditions presented in Sec. II. It has been pointed out that inhomogeneous field distributions can be described by an effective uniform electric field and can therefore be treated within the TDFF approach [28]. However, the phase of the TDFF line shape is altered compared to the uniform case.

In order to show the applicability of the laminar approach for inhomogeneous fields, Fig. 3(a) shows an ER spectrum (blue circles) which has been simulated for a single interface between a half-space of air and of CIGS. The simulation assumes an electro-optic energy of $\hbar\theta_1 = 5$ meV at the interface and a linear decrease of the electric field over a width of the SCR of $d_{SCR,1} = 150$ nm, hence an inhomogeneous field. For the dielectric function of CIGS, the CPPB oscillator

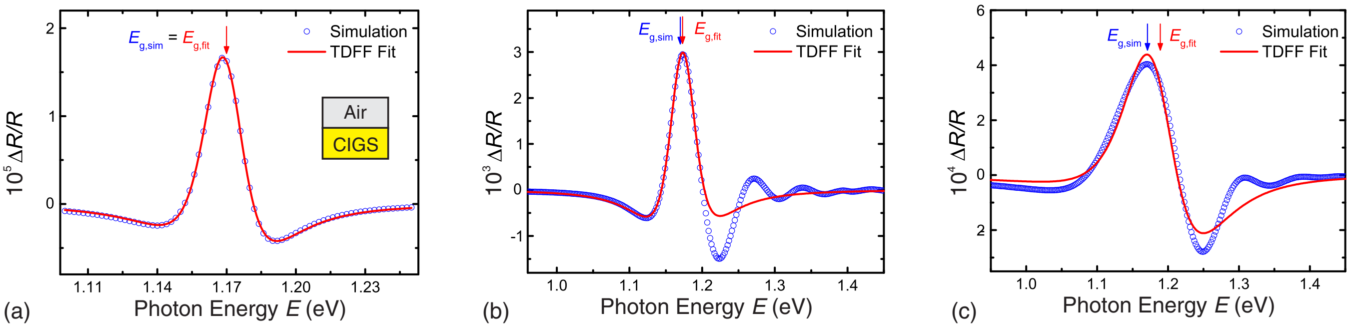

FIG. 3. (Color online) Simulated ER spectrum (blue) and TDFF fit (red) for a single CIGS interface [inset of (a)] and a single contributing optical transition. In (a) modulation occurs from zero field within the low-field limit while in (b) the low-field limit is exceeded. A TDFF fit can estimate the band gap in good agreement even though in (b) the FKOs cannot be described by a TDFF. In (c) an intrinsic field with realistic values for the electro-optic energy is implemented. In this case the simulated data deviates from the TDFF line shape and the fit parameter for $E_{g,sim}$ differs from the input parameter by 19 mV.

has been set to an energy of $E_{g,sim} = 1.170$ eV. For the change of the dielectric function due to $\hbar\theta_1$ a single optical transition at $E_{g,sim}$ with a broadening parameter of $\Gamma_{sim,1} = 20$ meV and an amplitude parameter of $B = 3.5$ is assumed. Since $\hbar\theta_1/\Gamma_{sim,1} \leqslant \sqrt[3]{4}/3$ this matches the conditions for the low-field approximation. As long as these conditions are met the exact values for $E_{g,sim}$ and $\Gamma_{sim,1}$ do not affect the following conclusions.

As evident from Fig. 3(a), the TDFF fit (red line) shows excellent agreement with the simulated data over the whole spectral range. The fit parameters are $E_{g,fit,1} = 1.170$ eV and $\Gamma_{fit,1} = 20$ meV, equal to the input parameters. The simulation routine therefore matches the expectations for the line shape and proves the applicability of the laminar approach for modeling an inhomogeneous field distribution in a half-space configuration. A similar simulation for a uniform field yields a spectrum with an altered phase of the line shape (not shown) as expected from theory.

If the electro-optic energy exceeds the low-field conditions, Franz-Keldysh oscillations (FKOs) appear in the electro-optic function. This case is treated in Fig. 3(b), which shows a $\Delta R/R$ spectrum with the same parameters as in Fig. 3(a) apart from an increased electro-optic energy of $\hbar\theta_2 = 40$ meV. Since $\hbar\theta_2/\Gamma_{sim,1} > \sqrt[3]{4}/3$, FKOs can be seen in the spectrum above E_g. Accordingly, a fit with a TDFF cannot reproduce the shape of the simulated data in this energetic region. However, since the TDFF captures the line shape below E_g relatively well, the band gap $E_{g,fit,2} = 1.173$ eV determined by the fit lies still close to the real value of $E_{g,sim} = 1.170$ eV. The broadening parameter $\Gamma_{fit,2} = 41$ meV on the other hand cannot be determined correctly by the TDFF. Electro-optic energies above the low-field limit therefore do not rule out a TDFF analysis of the spectra for the determination of E_g *a priori*. This, however, presumes that reflection takes place at a single interface, modulation occurs from zero field conditions, and optical transitions are sufficiently separated in energy space. Furthermore, in this case the FKOs must not be confused with contributions from additional transitions.

As previously discussed, for a real solar cell the modulation by an external electric field F_e does not occur from flat-band conditions. Therefore, we now consider the internal electric field F_i, since it is not part of the assumptions for the TDFF approximation. By repeating Aspnes's derivation for $\Delta\epsilon$ in the low-field limit, one can show that $\Delta\epsilon \propto \frac{\partial^3}{\partial E^3}(E^2\epsilon)$ still holds under the existence of F_i. However, when checking for the low-field conditions via $|\hbar\theta|/\Gamma \leqslant \sqrt[3]{4}/3$, the *full* field $F = F_i + F_e$ has to be used for the calculation of $\hbar\theta$. The full field might therefore be strong and exceed low-field conditions even if the modulating field is weak. Furthermore, the change in the width of the SCR might cause deviations from the TDFF line shape, because it is not taken into account in the low-field approximation.

Figure 3(c) shows a simulated ER spectrum (blue circles) for a CIGS layer with similar parameters to the one shown in Fig. 2. By estimating $\mu \approx 0.08m_e$ with m_e being the electron mass [35], $\hbar\theta_3 = 36$ meV and $d_{SCR,3} = 150$ nm without external field and $\hbar\theta_4 = 50$ meV and $d_{SCR,4} = 300$ nm with external field were assumed. The same values for $E_{g,sim}$ and B were used as above. From the width of the line shapes in actual ER measurements on CIGS solar cells $\Gamma_{sim,2}$ was estimated to be 60 meV. Since $|\hbar\theta_3|/\Gamma > \sqrt[3]{4}/3$, low-field conditions are exceeded and deviations from the TDFF line shape can be expected. Accordingly, the simulated data in Fig. 3(c) shows FKOs above the band gap. It can also be seen that the fitted curve (red) does not coincide with the simulated data so that the parameter $E_{g,fit,2} = 1.189$ eV deviates from $E_{g,sim}$ by 19 meV. The parameter $\Gamma_{fit,2} = 81$ meV also deviates from $\Gamma_{sim,2}$ by 21 meV.

We note that for lower doping concentrations, i.e., lower internal fields, the fits deviate less from the simulated data, even though for lower doping concentrations the change in d_{SCR} is larger. We therefore conclude that the quality of a TDFF fit for ER spectra of thin-film solar cells is mainly dominated by the doping concentration of the absorber layer. However, the physical reason that prohibits an accurate determination of E_g is not the existence of a high modulating field alone [see Fig. 3(b)], but the additional existence of a high intrinsic field in the SCR.

C. Interference effects in electroreflectance spectra

Additional to the electric field effects, the stratified nature of thin-film solar cells has to be taken into account. CIGS solar cells typically use a ZnO window layer to collect the

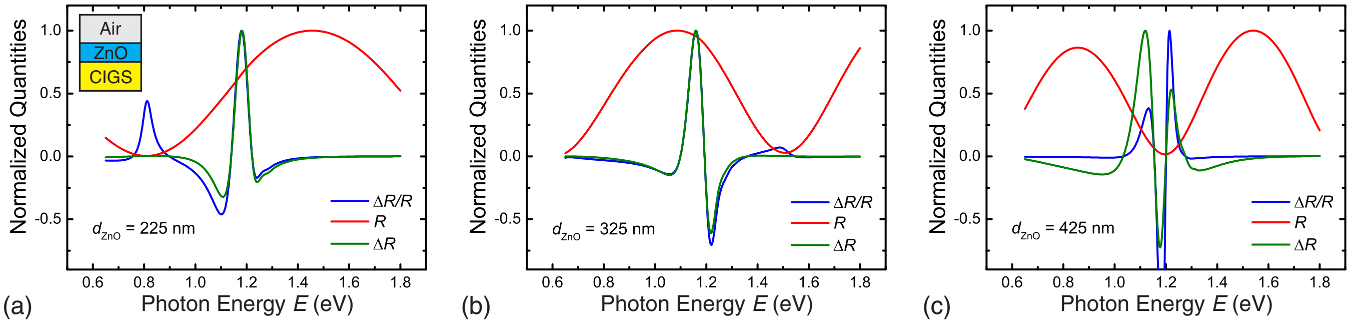

FIG. 4. (Color online) Simulated $\Delta R/R$, R, and ΔR signal for a CIGS half-space with low doping concentration and a ZnO window layer of varying thickness [see inset in (a)]. For a thickness of (a) $d_{\mathrm{ZnO},1} = 225$ nm and (b) $d_{\mathrm{ZnO},2} = 325$ nm the interference minimum in R lies energetically far away from the band gap. $\Delta R/R$ and ΔR both show a TDFF-like line shape and differ only in their phase parameter. For a thickness of (c) $d_{\mathrm{ZnO},3} = 425$ nm the interference minimum in R lies energetically close to the band gap. $\Delta R/R$ and ΔR both show strong deviations from the TDFF line shape.

electrons, because ZnO, being a wide band gap semiconductor, is transparent to light in the visible range. Both the air/ZnO and the ZnO/CIGS interface exhibit a contrast in the dielectric function so that part of the light is reflected at the respective interface. Since the thickness d_{ZnO} of such a window layer is typically in the order of several hundred nanometers, the ZnO layer causes interference oscillations in the reflection signal. The interference condition is not only determined by d_{ZnO}, but also by the phase shift introduced at the reflective interfaces. The modulation of the dielectric function of CIGS therefore directly affects the interference condition. It has already been pointed out by Aspnes that interferences in R can cause rapid changes in the Seraphin coefficients and therefore drastic distortions in ER signals [15]. This effect will be investigated in the following for ZnO window layers.

CIGS half-spaces with a low doping concentration and a ZnO window layer with three different thicknesses of 225, 325, and 425 nm, respectively, are examined. Figure 4 shows the simulated $\Delta R/R$ (blue), R (red), and ΔR (green) signal for each thickness. The R signals show interference oscillations, the frequency of which depends on the ZnO layer thickness d_{ZnO}.

For $d_{\mathrm{ZnO},1} = 225$ nm [Fig. 4(a)] and $d_{\mathrm{ZnO},2} = 325$ nm [Fig. 4(b)] the interference minimum in R lies energetically far away from E_g. In this case, ΔR shows a TDFF-like line shape at E_g. This is also true for $\Delta R/R$. However, those parts of the $\Delta R/R$ spectrum which lie energetically close to the interference minimum are amplified. The normalization of ΔR to R is usually done to cancel out instrument responses in the ER signal, assuming that ΔR and R scale proportionally to each other. The amplification of $\Delta R/R$ in these graphs shows that for variations in the measured R which are not caused by the measurement setup but by the spectral reflectivity of the sample itself, ΔR and R do not necessarily scale proportional to each other.

Furthermore, the phase of the line shape in ΔR and therefore also in $\Delta R/R$ changes depending on the energetic position of E_g in the interference pattern and thus the ZnO layer thickness.

For $d_{\mathrm{ZnO},3} = 425$ nm [Fig. 4(c)] however, the interference minimum in R lies in the close vicinity of E_g. In this case the line shape of ΔR—and in consequence $\Delta R/R$—is heavily distorted around E_g so that it does not resemble a TDFF anymore. This is especially due to an increased amount of zero crossings, a characteristic that cannot be represented by a simple TDFF line shape with a maximum of two zero crossings in Eq. (5). In a pure TDFF interpretation of a $\Delta R/R$ spectrum, an increased amount of zero crossings would indicate that more than one optical transition is present in this energetic region. We note that such an interpretation would especially seem natural in a semiconductor for which additional optical transitions can be expected due to slightly splitted valence bands. This is, e.g., the case for $\mathrm{CuInSe_2}$, in which the crystal-field splitting of the valence band is as low as 5 meV [24]. In summary, Fig. 4 shows that the line shape of $\Delta R/R$ is not solely determined by the dielectric function of the absorber layer, but also by the layer structure of the respective sample. This is the core problem to be faced when applying MS to layered systems.

The metallic Mo back contact of chalcopyrite thin-film solar cells represents another reflective interface. The light reflected at this interface interferes with the light reflected at the air/ZnO and the ZnO/CIGS interface and therefore causes further interferences in the reflection signal. This can be seen in Fig. 5, which shows $\Delta R/R$, R, and ΔR for a CIGS layer on a Mo half-space. The ZnO window layer is not considered for simplicity. The CIGS layer has a thickness of 2200 nm and is followed by a rough CIGS/Mo layer of 600 nm thickness as described in Sec. III C. The same parameters for the electric field and the optical transition as in Fig. 4 are assumed.

The interferences in R can only be seen on the low-energy side of E_g since above E_g light is absorbed in the CIGS layer. The rough implementation of the CIGS/Mo interface lowers the amplitude of the interference oscillations below E_g and increases the constant reflection above E_g. ΔR and $\Delta R/R$ exhibit oscillations below E_g with the same frequency as in R. Because of the broadening of the oscillator line shape, the low energy flank of the line shape lies in the energetic region of the interferences and therefore gets distorted. Without an additional ZnO layer the high energy flank of the oscillator line shape lies in a region of constant reflection and therefore remains unchanged.

The physical origin of the oscillations in ΔR caused by the Mo back contact is slightly different from that of the oscillations caused by the ZnO window layer. While for the latter the reflected light experiences the modulating effect

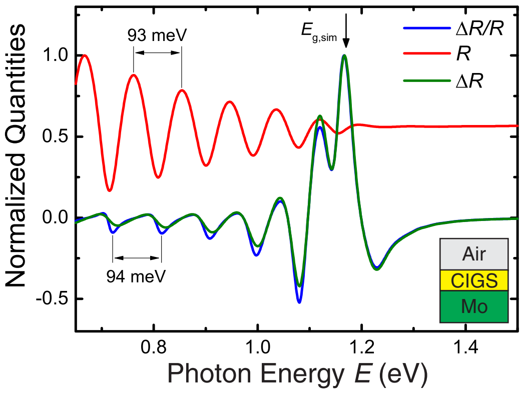

FIG. 5. (Color online) Simulated $\Delta R/R$, R, and ΔR signal for a CIGS layer on a Mo half-space (see inset). Interferences appear in R below the band gap. Oscillations with the same periodicity can be seen in ΔR and $\Delta R/R$. These extend into the energetic region of the oscillator line shape and distort the signal around the band gap.

only via the modulated reflection coefficient at the ZnO/CIGS interface, the light reflected at the Mo back contact propagates twice through the whole CIGS layer. A change in the dielectric function of the CIGS is therefore equivalent to a change of the length of the interference space itself.

The interference oscillations in ΔR, though exhibiting the same frequency, are shifted with respect to the oscillations in R. Therefore, they do not cancel out in $\Delta R/R$.

As it is the case for the ZnO window layer, the distortion of the $\Delta R/R$ line shape causes features which cannot be explained by a single TDFF oscillator. This additional structure could again easily be mistaken for a structure caused by further optical transitions. We conclude that in the presence of interference oscillations in R, spectra have to be interpreted very carefully—especially when relying on the TDFF line shape.

D. Fitting of measured data by transfer matrix algorithm

Finally, we present ER measurements of a CIGS thin-film solar cell with a Ga content (GGI) of $[\mathrm{Ga}]/([\mathrm{Ga}]+[\mathrm{In}]) \approx 0.23$ and a Cu content (CGI) of $[\mathrm{Cu}]/([\mathrm{Ga}]+[\mathrm{In}]) \approx 0.82$ at the buffer/absorber interface. The values have been determined by secondary neutral mass spectrometry (SNMS) at an adjacent cell on the same sample.

The measured reflection spectrum of the solar cell at an angle of incidence of 20° and an angle of detection of 20° is shown in Fig. 6(a) with blue circles. The measured values have first been corrected regarding instrument response by using a reflection spectrum taken from a gold mirror, which shows a reflectivity close to unity in the spectral region of interest. Interference oscillations are clearly visible in the lower energetic region and are quickly damped towards higher energies. The measured $\Delta R/R$ spectrum in Fig. 6(b) shows an oscillatory pattern in the lower energetic region and a pronounced derivativelike line shape at around 1.17 eV. For the high-energy region the signal from the InGaAs photodiode has been merged with the signal from the Si photodiode. At around 1.4 eV, a further broad line shape can be seen. The oscillations in R and $\Delta R/R$ at lower energies are due to the reflection at the Mo back contact as discussed before. The derivativelike line shape is attributed to the combined A and B transition at E_g, while the second line shape is assigned to the spin-orbit split-off band.

A manual fit to the measured data by means of the TMM algorithm for R as well as simultaneously $\Delta R/R$ is shown in red for both graphs. The simulated layer stack consists of air/ZnO/CIGS/Mo with a rough layer at every interface. The thicknesses have been adjusted to match the oscillation pattern in R solely. The resulting thicknesses agree satisfactorily with values determined by SNMS considering the phenomenology of the implementation of interface roughness in this simulation. The latter is also expected to cause the deviations between the amplitudes in the measured and simulated signal seen in Fig. 6(a). Particularly, scattering at surface roughness is not taken into account in our TMM simulation. In our experimental setup, however, scattered light is partly detected as well leading to a damping of the oscillations in the experimental data.

In order to manually fit the $\Delta R/R$ spectrum, the electrical properties of the SCR were set to $\hbar\theta_5 = 25$ meV, $d_{\mathrm{SCR},5} = 100$ nm for the unmodulated and $\hbar\theta_6 = 40$ meV, $d_{\mathrm{SCR},6} = 150$ nm for the modulated case, respectively. Such a high electro-optic energy corresponds to a high doping concentration, an assumption which is reasonable for a copper poor sample. This is due to copper vacancies which act as acceptors [36].

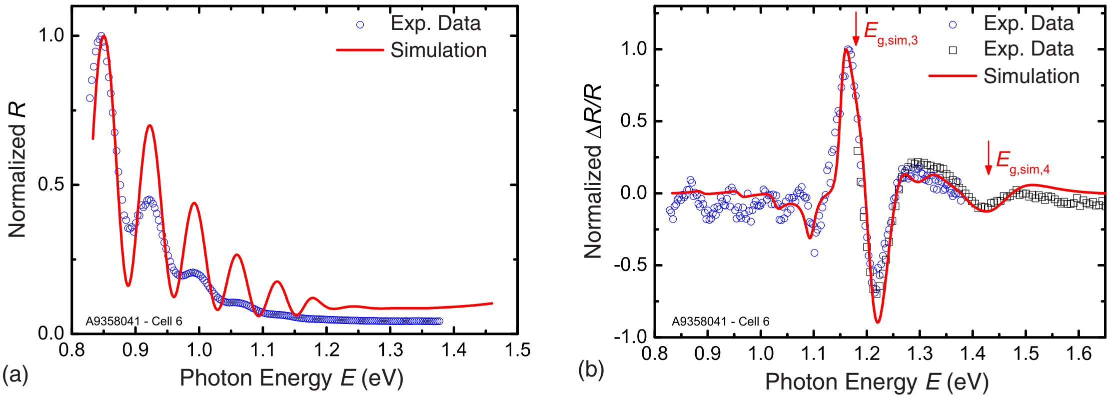

FIG. 6. (Color online) Measured (a) R and (b) $\Delta R/R$ signal of a CIGS solar cell and manual fit of the data by TMM. In (b) blue circles and black squares represent data measured by an InGaAs or Si photodiode, respectively. The simulation reproduces the positions of minima and maxima as well as the oscillator phase accurately.

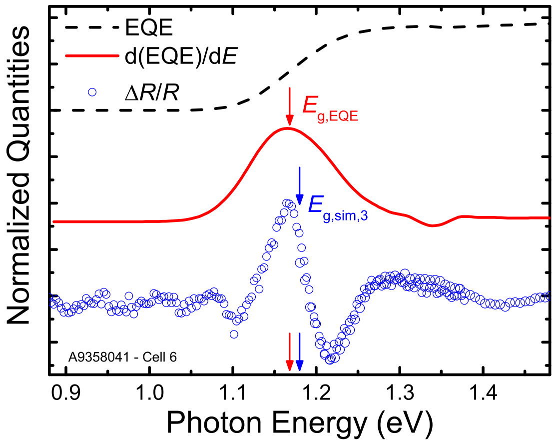

FIG. 7. (Color online) Comparison of ER and EQE data of the CIGS solar cell from Fig. 6. There is an offset between the data sets for better visibility. The EQE curve slowly decays below the band gap indicating the existence of tail states. The maximum of the first derivative of the EQE curve gives a band gap value of $E_{\mathrm{g,EQE}} = 1.171$ eV lying closely below the value $E_{\mathrm{g,sim,3}} = 1.180$ eV determined by the manual fit of ER data in Fig. 6(b).

The line shape at E_{g} was modeled by an optical transition at $E_{\mathrm{g,sim,3}} = 1.180$ eV, with broadening parameter $\Gamma_{\mathrm{sim,3}} = 46$ meV and amplitude $B_3 = 3.5$. Since the plateau above E_{g} could not be modeled by this single optical transition alone, a second transition was introduced with $E_{\mathrm{g,sim,4}} = 1.430$ eV, $\Gamma_{\mathrm{sim,4}} = 110$ meV, and amplitude $B_4 = 4.5$. We empirically estimate an accuracy of ±6 meV for these transition energy values based on a variation of the respective parameters and subsequent comparison with the measured data. We note that these two transitions are energetically separated by more than $\Gamma_{\mathrm{sim,4}}$, i.e., it is expected that such transitions can separately be resolved in an ER measurement.

The overall line shape of the simulated $\Delta R/R$ matches well with the measured data. In particular, the energetic positions of minima and maxima as well as the phase of the line shape around E_{g} show good agreement. Furthermore, the choice of layer thicknesses due to the R data also determines the minima of the oscillations in $\Delta R/R$ below E_{g} correctly. Deviations are due to the deviations in R caused by interface roughness which consequently also results in deviations in $\Delta R/R$. Furthermore, our CIGS model neglects possible states lying closely below E_{g} which could also be affected by the modulation and therefore enhance the measured ER signal in this energetic region.

Figure 7 shows a comparison between the EQE (black) and the ER (blue) of the same CIGS solar cell. It can be seen from the EQE curve that the absorption is smeared out rather broadly around E_{g}. This points towards the existence of tail states with a nonvanishing density below E_{g} [37].

The inflection point of the EQE data, i.e., the maximum of the first derivative with respect to the photon energy (Fig. 7 in red), can be used as an estimate for the band gap [19]. In our case fitting a Gaussian peak function to the data yields an estimated value of $E_{\mathrm{g,EQE}} = 1.171$ eV in close agreement with $E_{\mathrm{g,sim,3}} = 1.180$ eV.

We note that the value for $E_{\mathrm{g,sim,3}}$ is higher than the fundamental band gaps typically reported in literature for a gallium fraction of 0.23 in samples with stoichiometry between Cu and the group III element by 40–70 meV [25,38,39]. It has, however, been reported that Cu deficiency leads to an increase of E_{g} [23,40,41].

We would also like to stress that the broadening of the fundamental transition at room temperature of $\Gamma_{\mathrm{sim,3}} = 46$ meV is by an order of magnitude larger than the crystal-field splitting between A and B valence bands and therefore does not allow us to resolve their respective transitions individually. Consequently, we explicitly do not use any multioscillator fitting for these two transitions thus avoiding artifacts due to line shape distortions in a stratified system, as mentioned above. This means that our value of $E_{\mathrm{g,sim,3}} = 1.180$ eV represents the energetic position of an effective optical transition, comprising both A and B transition.

Depending on the publication considered, the C transition due to the spin-orbit split-off valence band is expected to lie in the range of $E_{\mathrm{C},0.23} = 1.27$–$1.52$ eV [25,38,39]. Our fitted value of $E_{\mathrm{g,sim,4}} = 1.43$ eV lies within this range [42].

The TMM therefore allows for a consistent description of both R and $\Delta R/R$ spectra of CIGS thin-film solar cells.

VI. CONCLUSIONS

Using TMM simulations, we investigated ER spectra of CIGS solar cells. The line shapes in these spectra can be subject to alterations compared to the line shapes in the typically assumed low-field conditions. It has been shown that the internal inhomogeneous electric field in the SCR combined with the change of its thickness during modulation leads to line shape deviations. In this case, depending on how large the doping concentration and therefore the intrinsic electric field is, a simple TDFF fit cannot determine the band gap or other critical points accurately anymore.

Simulations of CIGS layers with ZnO window layers or Mo back contacts, respectively, showed that interference effects in the reflection signal introduce further line shape distortions in the ΔR signal, which are not canceled out in the normalized quantity $\Delta R/R$. These distortions are particularly detrimental if the optical transition lies in the close energetic vicinity of a minimum in R. In this case, further zero crossings in $\Delta R/R$ can be induced. These distorted line shapes can easily resemble a contribution from several optical transitions lying energetically close to each other. We therefore strongly recommend to use multioscillator fits for spectra taken from stratified systems with great caution.

We have finally shown that the TMM approach is able to reproduce the main characteristics of a measured ER spectrum from a CIGS solar cell with a GGI of 0.23 and a CGI of 0.82. This allowed us to determine an effective oscillator for the A and B transition at 1.18 eV and a broad oscillator for the C transition at 1.43 eV.

ACKNOWLEDGMENTS

We acknowledge financial support from the Karlsruhe School of Optics and Photonics (KSOP) and the Carl-Zeiss-Foundation. We also thank the Zentrum für Sonnenenergie- und Wasserstoff-Forschung Baden-Württemberg for providing the solar cell sample and the SNMS data.

[1] P. Jackson, D. Hariskos, R. Wuerz, O. Kiowski, A. Bauer, T. M. Friedlmeier, and M. Powalla, Phys. Status Solidi R **9**, 28 (2015).

[2] D. Aspnes, Surf. Sci. **37**, 418 (1973).

[3] B. O. Seraphin and N. Bottka, Phys. Rev. **145**, 628 (1966).

[4] A. Grau, T. Passow, and M. Hetterich, Appl. Phys. Lett. **89**, 202105 (2006).

[5] F. Pollak and H. Shen, Mat. Sci. Eng. R **10**, xv (1993).

[6] M. Hetterich, A. Grau, A. Y. Egorov, and H. Riechert, J. Appl. Phys. **94**, 1810 (2003).

[7] M. Hetterich, A. Grau, A. Y. Egorov, and H. Riechert, J. Phys.-Condens. Mat. **16**, S3151 (2004).

[8] J. L. Shay and H. M. Kasper, Phys. Rev. Lett. **29**, 1162 (1972).

[9] J. L. Shay, B. Tell, H. M. Kasper, and L. M. Schiavone, Phys. Rev. B **5**, 5003 (1972).

[10] D. E. Aspnes, Phys. Rev. Lett. **28**, 913 (1972).

[11] S. Theodoropoulou, D. Papadimitriou, A. G. Mamalis, D. E. Manolakos, R. Klenk, and M.-C. Lux-Steiner, Semicond. Sci. Tech. **22**, 933 (2007).

[12] C. Krämmer, C. Huber, C. Zimmermann, M. Lang, T. Schnabel, T. Abzieher, E. Ahlswede, H. Kalt, and M. Hetterich, Appl. Phys. Lett. **105**, 262104 (2014).

[13] O. Kiowski, W. Witte, M. Hetterich, and M. Powalla, IEEE J. Photovolt. **4**, 285 (2014).

[14] F. Pollak, *Modulation Spectroscopy of Semiconductors and Semiconductor Microstructures*, edited by M. Balkanski, Handbook on Semiconductors, Vol. 2: Optical Properties of Semiconductors (North-Holland, Amsterdam, 1994).

[15] D. E. Aspnes, J. Opt. Soc. Am. **63**, 1380 (1973).

[16] D. Aspnes, *Modulation Spectroscopy/Electric Field Effects on the Dielectric Function of Semiconductors*, edited by M. Balkanski, Handbook on Semiconductors, Vol. 2: Optical Properties of Semiconductors (North-Holland, Amsterdam, 1980).

[17] D. E. Aspnes, Phys. Rev. **153**, 972 (1967).

[18] R. A. Batchelor, A. C. Brown, and A. Hamnett, Phys. Rev. B **41**, 1401 (1990).

[19] T. Gokmen, O. Gunawan, T. K. Todorov, and D. B. Mitzi, Appl. Phys. Lett. **103**, 103506 (2013).

[20] M. C. Troparevsky, A. S. Sabau, A. R. Lupini, and Z. Zhang, Opt. Express **18**, 24715 (2010).

[21] D. W. Lynch and W. Hunter, in *Handbook of Optical Constants of Solids*, edited by E. D. Palik (Academic, Burlington, VT, 1997), pp. 306–313.

[22] J. A. Woollam Co., Inc., WVASE32 - refractive index materials database, 2010.

[23] S. Minoura, K. Kodera, T. Maekawa, K. Miyazaki, S. Niki, and H. Fujiwara, J. Appl. Phys. **113**, 063505 (2013).

[24] J. L. Shay and B. Tell, Surf. Sci. **37**, 748 (1973).

[25] M. I. Alonso, M. Garriga, C. D. Rincón, E. Hernández, and M. León, Appl. Phys. A **74**, 659 (2002).

[26] D. Aspnes, Phys. Rev. B **10**, 4228 (1974).

[27] D. J. Hall, T. J. C. Hosea, and D. Lancefield, J. Appl. Phys. **82**, 3092 (1997).

[28] D. Aspnes and A. Frova, Solid State Commun. **88**, 1061 (1993).

[29] P. L. Jackson and E. G. Seebauer, J. Appl. Phys. **69**, 943 (1991).

[30] R. Kuz'menko, A. Ganzha, É. Domashevskaya, V. Kircher, and S. Hildebrandt, Semiconductors **34**, 1045 (2000).

[31] J. P. Estrera, W. M. Duncan, and R. Glosser, Phys. Rev. B **49**, 7281 (1994).

[32] K. Orgassa, Coherent optical analysis of the ZnO/CdS/Cu(In,Ga)Se_2 thin film solar cell, Ph.D. thesis, Universität Stuttgart, 2004.

[33] T. Wada, N. Kohara, S. Nishiwaki, and T. Negami, Thin Solid Films **387**, 118 (2001).

[34] M. Burgelman, P. Nollet, and S. Degrave, Thin Solid Films **361**, 527 (2000).

[35] C. Persson, Appl. Phys. Lett. **93**, 072106 (2008).

[36] R. Scheer and H.-W. Schock, *Chalcogenide Photovoltaics: Physics, Technologies, and Thin Film Devices* (Wiley-VCH, Berlin, 2011).

[37] J. Mattheis, U. Rau, and J. H. Werner, J. Appl. Phys. **101**, 113519 (2007).

[38] P. Paulson, R. Birkmire, and W. Shafarman, J. Appl. Phys. **94**, 879 (2003).

[39] A. Kindyak, V. Kindyak, and Y. Rud, Semiconductors **31**, 882 (1997).

[40] S.-H. Han, F. S. Hasoon, J. W. Pankow, A. M. Hermann, and D. H. Levi, Appl. Phys. Lett. **87**, 151904 (2005).

[41] S.-H. Han, F. S. Hasoon, H. A. Al-Thani, A. M. Hermann, and D. H. Levi, J. Phys. Chem. Solids **66**, 1895 (2005).

[42] An independent confirmation by EQE for our sample is not possible since the low absorption of the C transition leads to a negligible contribution to the EQE spectrum. Indeed, it is a strong advantage of modulation spectroscopy techniques such as ER that this transition can easily be detected.